Noninvasive imaging of liposomal delivery of superparamagnetic iron oxide nanoparticles to orthotopic human breast tumor in mice

Yoshinori Kato[#,1,2,3], **Wenlian Zhu**[#,1], **Marina V. Backer**[4], **Christopher C. Neoh**[1], **Sudath Hapuarachchige**[1], **Susanta K. Sarkar**[5], **Joseph M. Backer**[4,*], and **Dmitri Artemov**[1,2,*]

[1]Division of Cancer Imaging Research, The Russell H. Morgan Department of Radiology and Radiological Science, The Johns Hopkins University School of Medicine, Baltimore, MD, USA

[2]Department of Oncology, The Sidney Kimmel Comprehensive Cancer Center, The Johns Hopkins University School of Medicine, Baltimore, MD 21205, USA

[3]Life Science Tokyo Advanced Research Center (L-StaR), Hoshi University School of Pharmacy and Pharmaceutical Science, Shinagawa-ku, Tokyo, JAPAN (Current affiliation)

[4]SibTech, Inc., Brookfield, CT 06804, USA

[5]CadenzaMed LLC, Wayne, PA 19087, USA

[#] These authors contributed equally to this work.

Abstract

Purpose—Magnetic resonance imaging (MRI) is widely used for diagnostic imaging in preclinical studies and in clinical settings. Considering the intrinsic low sensitivity and poor specificity of standard MRI contrast agents, the enhanced delivery of MRI tracers into tumors is an important challenge to be addressed. This study was intended to investigate whether delivery of superparamagnetic iron oxide nanoparticles (SPIONs) can be enhanced by liposomal SPION formulations for either "passive" delivery into tumor via the enhanced permeability and retention (EPR) effect or "active" targeted delivery to tumor endothelium via the receptors for vascular endothelial growth factor (VEGFRs).

Methods—*In vivo* MRI of orthotopic MDA-MB-231 tumors was performed on a preclinical 9.4T MRI scanner following intravenous administration of either free/non-targeted or targeted liposomal SPIONs.

Results—*In vivo* MRI study revealed that only the non-targeted liposomal formulation provided a statistically significant accumulation of SPIONs in the tumor at four hours post-injection. The EPR effect contributes to improved accumulation of liposomal SPIONs in tumors compared to the presumably more transient retention during the targeting of the tumor vasculature via VEGFRs.

---

[*]Correspondence to: <u>Dmitri Artemov, Ph.D.</u>, 720 Rutland Avenue, Traylor 217, Baltimore, MD 21205, USA, Phone: 410-614-2703, Fax: 410-614-1948, dartemo2@jhmi.edu.

Conclusions—A non-targeted liposomal formulation of SPIONs could be the optimal option for MRI detection of breast tumors and for the development of therapeutic liposomes for MRI-guided therapy.

Keywords

liposomes; magnetic resonance imaging (MRI); passive targeting; single-chain vascular endothelial growth factor (scVEGF); superparamagnetic iron oxide nanoparticles (SPIONs)

INTRODUCTION

Magnetic resonance imaging (MRI) is a clinical multiparametric modality that provides anatomical and functional information non-invasively, with high spatial resolution and with no ionizing radiation. The use of paramagnetic contrast agents further enhances the sensitivity of MRI. Furthermore, these contrast agents can be adapted for visualization of drug delivery, drug release, and intratumoral distribution of nanocarriers [1-3]. Superparamagnetic iron oxide nanoparticles (SPIONs) are the so-called T_2 agents that shorten transverse (T_2) relaxation time for water protons and generate hypointense signals in T_2- and T_2*-weighted MR images. SPIONs have good MRI sensitivity and biocompatibility. They are readily taken up by the liver reticuloendothelial system, providing a facile method of hepatic imaging. Unfortunately, rapid clearance of SPIONs hinders their use for tumor imaging, except for liver tumors. Therefore, the development of formulations that could provide more sustainable tumor uptake of SPIONs is an important goal in the clinic. In this study, we explored two approaches to enhance the tumor uptake of SPIONs. In the first approach, SPIONs were encapsulated in liposomes to allow for passive tumor accumulation via the enhanced permeability and retention (EPR) effect. The EPR effect is based on the leakiness of the tumor vasculature [4], which allows for passive extravasation of liposomes through the vascular wall with subsequent retention in the perivascular space within one or two layers of tumor subendothelial cells [5-7]. In the second approach, the above liposomes encapsulated with SPIONs were further decorated with scVEGF, a recombinant single-chain version of vascular endothelial factor to target the VEGF receptors (VEGFRs) that overexpressed on endothelial cells in the growing tumor vasculature [8]. VEGFRs are readily accessible to contrast agents from the bloodstream, allowing for selective tumor accumulation of scVEGF-driven imaging probes, such as nuclear tracers, fluorescent liposomes and ultrasound microbubbles [8-10]. We, therefore, reasoned that tethering scVEGF to SPIONs-encapsulated liposomes would improve the accumulation of the liposomal MRI probe in the vasculature of a growing tumor. Of note, another attractive endothelial target, $\alpha_v\beta_3$ integrins, has been explored previously for MRI of the tumor vasculature with paramagnetic MRI probes, such as polymerized liposomes [11], and emulsions [12] decorated with cyclic RGD peptides.

In this study, in addition to SPIONs, a gadolinium-based MRI contrast agent, Gadodiamide (Omniscan™), was also co-encapsulated into the liposomes, and termed Lip(Gd/Fe), to monitor the stability of liposome *in vivo* using a dual-contrast method [1, 2]. MR imaging was used to assess the extent to which liposomal formulation improves the delivery of

SPIONs to orthotopic human breast tumor xenografts via passive EPR and active VEGFR-targeting approaches.

METHODS

Materials

Distearoyl phosphatidylcholine (DSPC), distearoyl phosphatidylethanolamine methoxy(polyethylene glycol) conjugate (DSPE-PEG$_{2000}$), cholesterol, and indocyanine green dye (ICG) were purchased from Sigma-Aldrich Co. (St. Louis, MO). scVEGF-PEG$_{3400}$-DSPE conjugate was prepared by site-specific conjugation of DSPE-PEG$_{3400}$-maleimide (Nektar Therapeutics) to [C4]-monothiol-scVEGF (SibTech, Inc. Brookfield, CT), using a four-fold molar excess of DSPE-PEG$_{3400}$-maleimide and 10 min incubation at room temperature. Phospholipids C was purchased from Wako Diagnostics (Richmond, VA). Omniscan™ (GE Healthcare, gadodiamide injection) was used as a T_1 contrast agent, and Feridex I.V.® (Bayer HealthCare Pharmaceuticals Inc., ferumoxides injectable solution) and nanomag®-D-spio (micromod Partikeltechnologie GmbH, Rostock, Germany) were used as T_2 contrast agents. All other solvents or chemicals were of reagent grade.

Cell Line and Animals

Triple-negative MDA-MB-231 human breast cancer cells that stably express firefly luciferase (MDA-MB-231/luc) were provided by SibTech, Inc. (Brookfield, CT), and cultured in DMEM supplemented with 10% FBS and 1% penicillin-streptomycin at 37°C with 5% CO_2. Female athymic nude mice were purchased from the NCI (Frederick, MD), and orthotopic MDA-MB-231/luc tumor models were established by inoculating 2×10^6 cells dispersed in 50 μL of 50% Matrigel™/Hanks' balanced salt solution into the mammary fat pad of the mice. All animal experiments with MDA-MB-231/luc were conducted according to protocols approved by the Johns Hopkins University Animal Care and Use Committee.

4T1/luc cells, a luciferase-expressing derivative of 4T1 mouse mammary carcinoma cells, were provided by SibTech, Inc. (Brookfield, CT), and cultured under the same conditions as MDA-MB-231/luc cells. To obtain orthotopic tumors, 1×10^5 4T1/luc cells in Hanks' solution were injected into mammary fat pad of seven week-old Balb/c female mice. All animal experiments with 4T1/luc cells were conducted by JMB and MVB at the University of Connecticut Health Center Animal Facilities (Farmington, CT) according to protocols approved by the University of Connecticut Health Center Animal Care and Use Committee.

Preparation of Liposomes

Liposomes (with or without PEGylated lipids) were prepared by lipid hydration with a mixture of Omniscan™ (500 μL), Feridex I.V.® (50 μL), and saline (450 μL), followed by extrusion in a manner similar to our previous report [1]. The lipid molar compositions of non-targeted liposomes (Lip(Gd/Fe)) and scVEGF-decorated liposomes (scVEGF-Lip(Gd/Fe)) were DSPC/DSPE-PEG$_{2000}$/cholesterol = 6.3/0.7/5.2, and DSPC/cholesterol = 6.3/5.2, respectively.

Fluorescence-labeled, ICG-loaded liposomes, (Lip(ICG)), were prepared as described recently [10]. Briefly, phospholipids and cholesterol in chloroform were mixed at the following molar percent ratio: DOPE(31):Cholesterol(33.5):DOPC(31):DOPE-PEG$_{2000}$(2.5) and evaporated under vacuum for one hour. To remove residual chloroform, cyclohexane was added to dry phospholipid/cholesterol film, vortexed for one minute, and evaporated under vacuum for one hour. ICG was added to dry lipids as a stock solution in methanol (5-7 mg/ml) and vortexed for one minute to ensure the efficient mixing of lipids/cholesterol film with the dye. Methanol was then evaporated under vacuum for 16 hours in the dark. Dry phospholipid/cholesterol/ICG film was hydrated in a buffer containing 10 mM HEPES (pH 7.2), 150 mM NaCl, and 0.2 mM EDTA, passed through three cycles of freezing at liquid nitrogen and thawing at 58°C, and 25-cycles of extrusion through 80-nm-pore-diameter polycarbonate membranes at 58°C. The resulting unilamellar liposomes were purified by size-exclusion chromatography on Sepharose 4B. The concentration of liposome-entrapped ICG was determined in methanol lysates by absorbance at 784 nm, using ICG stock solution in methanol as a standard.

Decoration of Lip(Gd/Fe), Lip(ICG), and Doxil® (clinically used doxorubicin-containing STEALTH liposomes) with scVEGF was achieved by post-insertion of scVEGF-PEG$_{3400}$-DSPE conjugate into a liposomal membrane, as previously described for different liposomal formulations [13, 14]. Briefly, the entire reaction mixture of [C4]-monothiol-scVEGF with DSPE-PEG$_{3400}$-maleimide was added to purified liposomes at an average scVEGF-to-phospholipid molar ratio of 1:150, and incubated for 12-14 hours at 37°C. scVEGF-decorated liposomes were purified from free protein by size-exclusion chromatography on Sepharose 4B. The concentration of scVEGF was determined by SDS-PAGE, with free scVEGF serving as a standard.

Characterization of Liposomes

The hydrodynamic diameter and zeta-potential of liposomes were determined by photon correlation spectroscopy (Malvern Instruments Ltd.). Iron and gadolinium contents were determined by inductively coupled plasma mass spectrometry (ICP-MS).

Immunohistochemistry

Double fluorescent staining for VEGF receptors and a pan-endothelial marker CD31 (PECAM) was conducted as previously described [19]. Briefly, tumor cryosections of 5-μm thickness were fixed with 1% formaldehyde (Polysciences) for 10 min at room temperature. Endogenous tissue peroxidase was quenched by a 10-min incubation in 1% peroxide, and endogenous biotin was blocked with an avidin-biotin blocking kit (Molecular Probes). After blocking in 5% normal rabbit serum, tissue was probed first with VEGFR-2 (Flk-1) rat monoclonal antibody (BD Pharmingen), followed by biotinylated, mouse tissue-absorbed anti-rat IgG developed in rabbits (Vector Laboratories), which was then coupled to streptavidin-peroxidase conjugate and visualized with AlexaFluor-488 using a tyramide amplification technique (TSA HRP-streptavidin Kit, Molecular Probes). Next, peroxidase was quenched by a one-hour incubation in 6% peroxide at room temperature, and VEGFR-2 stained sections were probed with either CD31 (PECAM, rat monoclonal antibody from BD Pharmingen) or VEGFR-1 (FLT1, rat monoclonal antibody from Santa Cruz) that were

visualized with a different dye, AlexaFluor-594, using the same tyramide amplification technique. Slides were mounted in medium for fluorescence, supplemented with DAPI for nuclear counterstaining (Vector Laboratories), and observed in a Zeiss Axiovert microscope with 20× objective.

In Vivo MRI

MR studies were performed on a horizontal bore, preclinical 9.4T Bruker Biospec spectrometer using a custom-built, single-turn solenoid coil. Mice were anesthetized with isoflurane (1% in oxygen), and the tumor was positioned within the coil. Anesthesia was maintained throughout the MRI experiment. T_2-weighted images of the tumors were acquired using the rapid acquisition with refocusing echoes (RARE) sequence before and after the intravenous administration of SPION-based contrast agents at a dose of 11 μmol eq. Fe/kg, with a repetition time (TR) of 4 s and four effective echo times (TE; 7, 21, 35, and 49 ms) to locate the SPIONs. Other parameters were as follows: isotropic field of view = 15 mm; matrix size of 128×128. To assess the stability of the liposomes, T_1-weighted images were acquired with the RARE sequence, using an effective TE of 7 ms and four TRs (0.5, 1, 2, and 8 s). Post contrast images were acquired at 30 minutes, four hours, and one day after the injection of the contrast agents.

T_2-weighted images were analyzed using custom-written software in the Interactive Data Language (IDL; Exelis Visual Information Solution). To provide quantitative comparison within the groups, an uptake index was calculated based on the hypointense pixels within the region-of-interest (ROI) by the Otsu's thresholding method, using the intensity of nearby muscle as a reference. Briefly, amplitudes of the images were reversed, and a binary tumor uptake mask was generated by multiple thresholding, relative to the reference amplitude, calculated as a mean signal from the muscle ROI. The mask value was set at 1 for the enhancing regions with the highest intensity after the amplitude reversal, and 0 everywhere else. The uptake index was calculated for the entire tumor (Image 1) using the following equation:

$$\text{Uptake index} = \text{total}\left(\text{image1} * \text{mask}\right) / \text{total}\left(\text{image1}\right)$$

Quantitative T_1 maps of the images were reconstructed using the IDL programming environment.

In Vivo Optical Imaging

The delivery of Lip(ICG) or scVEGF-Lip(ICG) to the MDA-MB-231/luc tumor was optically monitored using an IVIS Spectrum Pre-clinical In Vivo Imaging System (PerkinElmer; Santa Clara, CA, USA). Images were acquired with excitation and emission wavelengths of 645/820 nm over time.

Therapeutic Experiment with Doxil®

Tumor-bearing Balb/c mice were randomized for treatment (*N*=4, each group) when orthotopically growing 4T1/luc tumors reached volumes of 50-100 mm³. Free doxorubicin, Doxil®, and scVEGF-decorated Doxil® were injected i.v. at 2 mg/kg of doxorubicin. The

control group received equivalent volumes of saline. Tumor sizes were measured with calipers every other day, starting at day 3 and finishing at day 12 post injection. Tumor volumes were calculated as $V = 0.52 \times L \times W \times H$, where L, W, and H are tumor length, width, and height.

Statistical Analysis

In the MRI study, five animals were used for nanomag®-D-spio, and six animals were used for Lip(Gd/Fe) and scVEGF-Lip(Gd/Fe) groups. Statistical comparison of uptake index was performed between the groups using a nonparametric Friedman ANOVA on StatPlus®:mac (AnalystSoft Inc., Alexandria, VA, USA). Differences between intratumoral accumulation of SPIONs in various groups and differences of tumor volumes between the groups in the therapeutic study were considered significant if the *P*-value was less than 0.05.

RESULTS

Preparation of SPION-Based Liposomal Probes

The physicochemical characteristics of liposomes loaded with MRI contrast agents are shown in Table 1. As expected, the hydrodynamic diameter of scVEGF-Lip(Gd/Fe) was slightly larger than that of Lip(Gd/Fe), and both liposomes had similar negative surface charges. The scVEGF content was 1.9 ± 0.3 μmol/mmol of lipids. The contents of gadolinium and iron in scVEGF-Lip(Gd/Fe) were lower than those in Lip(Gd/Fe), which was attributed to the extra steps required for the post-insertion decoration with scVEGF.

VEGFR-2 is Predominantly Expressed in the Tumor Vasculature in Matrigel-Supported Orthotopic MDA-MB-231/luc Model

To assess liposomal SPION formulations *in vivo*, we employed Matrigel-supported orthotopic MDA-MB-231/luc tumors. It is widely accepted that orthotopic inoculation acts synergistically with Matrigel to accelerate tumor growth [15]. To characterize the state of the vasculature and the prevalence of VEGFRs in the tumor endothelium in this Matrigel-supported tumor model, we used immunohistochemical analysis of VEGFRs and pan-endothelial marker CD31. We found that the majority of VEGFR-2 co-localizes with pan-endothelial marker CD31 (Figure 1, top panels), whereas VEGFR-1 has little, if any, co-localization with predominantly endothelial VEGFR-2 (Figure 1, bottom panels). These results indicate that VEGFR-2 is expressed on tumor endothelial (CD31-positive) cells in this tumor model, and is the primary target for specific binding of scVEGF-Lip(Gd/Fe) from the bloodstream.

In Vivo MRI Experiments

Representative T_2-weighted MR images of orthotopic MDA-MB-231/luc tumors before and at four and 24 hours after intravenous administration of the free or liposomal SPIONs are shown in Figure 2. The injection dose was based on the absolute amount of iron in SPIONs, regardless of the liposomal preparation. There was a highly variable accumulation of free and liposomal SPIONs in the tumors at four hours, as demonstrated by the T_2-weighted image signal intensity decline shown in Figure 2. Some of these signal declines were still present at 24 hours for all formulations, Figure 2, right column. For longitudinal

characterization of tumor uptake of SPIONs in individual tumors, we used the uptake index as defined in the Methods section. An analysis of longitudinal changes in the uptake index revealed significant variations between individual animals in each experimental group, including the presence of mild and severe outliers (Figure 3A). Nevertheless, we found that the median uptake index for free SPIONs was not statistically different from that of the pre-contrast images. However, for liposomal SPIONs formulations, the highest uptake index was observed at four hours, although the difference from the pre-contrast level was statistically significant only for the group injected with Lip(Gd/Fe).

We also analyzed each representative slice of MRI images in the Lip(Gd/Fe) and scVEGF-Lip(Gd/Fe) groups for the prevalence of hypointense pixels at the 80th percentile, which reflects areas with the highest accumulation of SPIONs. As shown in Figure 3B, this parameter provided additional discrimination between groups, whereas accumulation in the Lip(Gd/Fe) group at four and 24 hours was statistically higher relative to pre-contrast or 30 min images, respectively, while in the scVEGF-Lip(Gd/Fe) group accumulation was higher only at four hours, followed by a decline to the pre-contrast level at 24 hours. The latter observation could be due to i) the loss of SPIONs by degradation of scVEGF-Lip(Gd/Fe); or ii) faster clearance of intact scVEGF-Lip(Gd/Fe) from the tumor area compared to untargeted liposomes.

The stability of liposomes was checked by T_1-weighted MRI, and shown in representative quantitative T_1-maps of tumors obtained at 0, 4, and 24 hours (Figure 4). A reduction in T_1 was observed in quantitative T_1 maps in tumor areas where Lip(Gd/Fe) was localized (Figure 4A) whereas no T_1 reduction was observed in the tumor of the mice that received scVEGF-Lip(Gd/Fe) (Figure 4B).

Taken together, these data indicated that untargeted Lip(Gd/Fe) provide for a better accumulation in, or slower clearance from, tumor than did similar liposomes targeted to VEGFRs on endothelial cells in the tumor vasculature.

In Vivo Optical Imaging

Our findings that non-targeted liposomal formulation of SPIONs provided better MRI enhancement than its liposomal counterpart targeting the VEGFRs was unexpected, as we recently reported the opposite effect in a shorter-term (five hours), longitudinal, near-infrared fluorescent tomography study with ICG-encapsulating liposomes [10]. In view of this discrepancy, we hypothesized that the imaging results with ICG-encapsulating liposomes might be attributable to ICG that leaked out of liposomes, rather than liposome-encapsulated ICG. We found that purified Lip(ICG) displayed a low level of fluorescence in PBS, due to self-quenching in liposomes. However, following a short incubation of Lip(ICG) in 5% human serum albumin, the fluorescent signal increased approximately four-fold (Figure 5). These results indicated that *in vivo* imaging with Lip(ICG) and scVEGF-Lip(ICG) might have been due to ICG that was released from liposomes, bound to blood proteins (such as albumin), and extravasated as an ICG-protein complex, which is much smaller in size than Lip(ICG). In this model, scVEGF-Lip(ICG) bound to VEGF receptors in the tumor vasculature might work as a local depot for ICG, which is gradually released from liposomes, and immediately forms a complex with serum albumin and is extravasated

through the tumor blood vessels as an ICG-albumin complex. Indeed, near-infrared fluorescent imaging demonstrated a stronger signal in the tumor area at 24 hours post-injection of scVEGF-Lip(ICG) compared to Lip(ICG) (Figure 6).

Targeting Therapeutic Liposomes

Since imaging data indicated that non-targeted liposomes accumulated in tumors more efficiently than liposomes targeted to VEGFRs, we tested whether the targeting affects the therapeutic potential of drug-loaded liposomes. The immune system is an important player in cancer chemotherapy [16]; therefore, to assess the therapeutic efficacy of drug-loaded liposomes, we employed 4T1/luc mouse breast carcinoma grown orthotopically in syngeneic immunocompetent BALB/c mice, using Doxil®, the clinically approved doxorubicin formulation in PEGylated liposomes as a control. Doxil® was further decorated with scVEGF and its therapeutic efficacy was compared to that of Doxil® or free doxorubicin. The predominant expression of VEGFR-2 receptors on tumor endothelial cells in this tumor model has been reported earlier [8]. As shown in Figure 7, both liposomal and free doxorubicin at the selected dosing of 2 mg/kg inhibited tumor growth; however, Doxil® was significantly more efficient than free doxorubicin, whereas scVEGF-Doxil® was not. In fact, scVEGF-Doxil® was significantly less efficient than untargeted Doxil.®

DISCUSSION

In this study, the delivery of SPIONs to MDA-MB-231/luc tumors was significantly improved by encapsulating the SPIONs into non-targeted liposomes, providing for their distinct visualization in the tumors by T_2-weighted MRI. As was reported for other liposomal formulations, the uptake of Lip(Gd/Fe) was, most likely, due to the EPR effect associated with a leaky tumor vasculature [4]. Interestingly, we found that the scVEGF-Lip(Gd/Fe) formulation targeted to VEGF receptors in the tumor vasculature was less efficient in MR imaging. Analysis of longitudinal images indicates that this might have been due to the more rapid clearance of SPIONs from the tumors, either by intratumoral degradation of scVEGF-Lip(Gd/Fe) or by the removal of intact scVEGF-Lip(Gd/Fe) from the tumor area.

The stability of liposomes *in vivo* was assessed with a dual MRI labeling approach, on the grounds that positive T_1 contrast becomes evident after the leakage of a free GdDTPA-BMA low-molecular-weight agent from ruptured liposomes and subsequent rapid diffusion of GdDTPA-BMA into areas beyond the T_2 effect of SPIONs [1, 2]. Although released SPIONs, which have a significantly shorter diffusion range *in vivo*, did not interfere with the calculation of T_1 values *in vivo* in our previous study [2], SPIONs intrinsically have a T_1 effect, in addition to a strong T_2 effect [17]. The areas where a reduction in T_1 values was observed (Figure 4A) were within the areas of T_2 negative enhancement, implying that the reduction in T_1 values was most likely caused by the high concentration of SPIONs, and not by GdDTPA-BMA released from the Lip(Gd/Fe). In contrast, no T_1 reduction was observed in the tumor with scVEGF-Lip(Gd/Fe), which could be attributed to the following: i) there was no degradation of scVEGF-Lip(Gd/Fe), thus the T_1 reduction was not detected; or ii) the intact scVEGF-Lip(Gd/Fe) was cleared from the tumor area, as discussed above. Overall, it

was difficult to evaluate the stability of the liposomes in this study because the tumor MRI enhancement of Lip(Gd/Fe) was dominated by the negative T_2 effect of SPIONs.

Our original hypothesis, based on our previous study with PET, SPECT, fluorescent, and ultrasound scVEGF-based tracers [9], was that scVEGF-Lip(Gd/Fe) would accumulate in tumors primarily via binding to readily accessible VEGFR-2 receptors, which might lead to receptor-mediated internalization. However, current MRI data indicate that this is not the case, and, in fact, such targeting to VEGF receptors may actually decrease the accumulation of the liposomes in tumors. Furthermore, in agreement with imaging data, VEGFR targeting also decreased the efficacy of therapeutic liposomes. Of note, recent detailed flow cytometry analysis of endothelial cells in MDA-MB-231 tumor xenografts revealed that the average number of VEGF receptors per endothelial cell was relatively low (8,200-15,000/cell for VEGFR-1 and 1,200-1,700/cell for VEGFR-2) [18]. However, a selected fraction of endothelial cells (10-20%) expresses significantly higher number of VEGF receptors (>100,000/cell), which is apparently sufficient for the successful deployment of scVEGF-based tracers for different imaging modalities in this model [8]. Furthermore, the relative abundance of VEGFR-2 in the tumor vasculature in Matrigel-supported MDA-MB-231/luc and in 4T1/luc models was demonstrated in this study (Figure 1) and elsewhere [8], respectively. Thus, to explain the lower imaging efficiency of VEGFR-targeted, compared to the non-targeted MRI liposomes, we hypothesize that VEGFRs on the tumor endothelium may act, in effect, as a barrier for targeted liposomes, which decreases the efficiency of EPR-mediated extravasation and accumulation. However, we cannot rule out the possibility that the decoration of liposomes with scVEGF could, by itself, change the ability of liposomes to extravasate. Interestingly, there are several reports that, in preclinical studies, non-targeted nanotherapeutics provide better therapeutic efficacy against tumors compared to targeted nanotherapeutics [19, 20]. However, our data with Lip(ICG) and scVEGF-Lip(ICG) indicate that endothelium-targeting might be beneficial for liposomes that carry a "leakable" cargo capable of serum protein binding, such as ICG.

Overall, our conclusion is that liposome encapsulation significantly improves the delivery and retention of SPIONs in tumors and that passively targeted SPION liposomes have significantly better accumulation in the tumor compared to VEGFR-targeted SPION liposomes and free SPIONs, as measured by MRI. Therefore, liposomal SPIONs can be considered a highly efficient platform for sensitive diagnostics and, if co-encapsulated with drugs, for the development of image-guided drug delivery.

ACKNOWLEDGMENT AND DISCLOSURES

ABBREVIATIONS

DAPI	4′,6-Diamidino-2-phenylindole
DOPC	1,2-Dioleoyl-*sn*-glycero-3-phosphocholine

DOPE	1,2-Dioleoyl-*sn*-glycero-3-phosphoethanolamine
DSPC	1,2-Distearoyl-*sn*-glycero-3-phosphocholine
DSPE-PEG$_{2000}$	1,2-Distearoyl-*sn*-glycero-3-phosphoethanolamine-N-[amino(polyethylene glycol)-2000
EPR	Enhanced permeability and retention
GdDTPA-BMA	Gadolinium-diethylenetriamine pentaacetic acid-bismethylamide
ICG	Indocynine green
scVEGF-Lip(ICG)	scVEGF-decorated Lip(ICG)
ICP-MS	Inductively coupled plasma mass spectrometry
IDL	Interactive data language
Lip(Gd/Fe)	Liposomes encapsulated with GdDTPA-BMA and SPIONs
Lip(ICG)	Liposomes encapsulated with indocynine green
MRI	Magnetic resonance imaging
PDI	Polydispersity index
PECAM	Platelet endothelial cell adhesion molecule
PET	Positron emission tomography
RARE	Rapid acquisition with refocusing echoes
ROI	Region-of-interest
scVEGF	Single chain vascular endothelial growth factor
scVEGF-Lip(Gd/Fe)	scVEGF-decorated Lip(Gd/Fe)
SDS-PAGE	Sodium dodecyl sulfate polyacrylamide gel electrophoresis
SPECT	Single photon emission computed tomography
SPIONs	Superparamagnetic iron oxide nanoparticles
T$_1$	Spin–lattice relaxation time
T$_2$	Transverse relaxation time
TE	Echo time
TR	Repetition time
TSA	Tyramide signal amplification
VEGFRs	Vascular endothelial growth factor receptors

REFERENCES

1. Kato Y, Artemov D. Monitoring of release of cargo from nanocarriers by MRI/MRSI: Significance of T_2/T_2* effect of iron particles. Magn Reson Med. 2009; 61(5):1059–65. [PubMed: 19253373]

2. Onuki Y, Jacobs I, Artemov D, Kato Y. Noninvasive visualization of *in vivo* release and intratumoral distribution of surrogate MR contrast agent using the dual MR contrast technique. Biomaterials. 2010; 31(27):7132–8. [PubMed: 20580427]

3. Kato, Y.; Pathak, AP. Combined contrast and therapeutic nanocarriers for oncologic MRI. In: Phillips, WT.; Goins, BA., editors. Nanoimaging. Pan Stanford Publishing Pte. Ltd.; Singapore: 2011. p. 1-17.

4. Matsumura Y, Maeda H. A new concept for macromolecular therapeutics in cancer chemotherapy: mechanism of tumoritropic accumulation of proteins and the antitumor agent smancs. Cancer Res. 1986; 46(12 Pt 1):6387–92. [PubMed: 2946403]

5. Jain RK. Vascular and interstitial barriers to delivery of therapeutic agents in tumors. Cancer Metastasis Rev. 1990; 9(3):253–66. [PubMed: 2292138]

6. Jain RK. Barriers to drug delivery in solid tumors. Sci Am. 1994; 271(1):58–65. [PubMed: 8066425]

7. Chauhan VP, Stylianopoulos T, Martin JD, Popovic Z, Chen O, Kamoun WS, Bawendi MG, Fukumura D, Jain RK. Normalization of tumour blood vessels improves the delivery of nanomedicines in a size-dependent manner. Nat Nanotechnol. 2012; 7:383–8. [PubMed: 22484912]

8. Backer MV, Levashova Z, Patel V, Jehning BT, Claffey K, Blankenberg FG, Backer JM. Molecular imaging of VEGF receptors in angiogenic vasculature with single-chain VEGF-based probes. Nat Med. 2007; 13(4):504–9. [PubMed: 17351626]

9. Anderson CR, Rychak JJ, Backer M, Backer J, Ley K, Klibanov AL. scVEGF microbubble ultrasound contrast agents: a novel probe for ultrasound molecular imaging of tumor angiogenesis. Invest Radiol. 2010; 45(10):579–85. [PubMed: 20733505]

10. Zanganeh S, Xu Y, Hamby CV, Backer MV, Backer JM, Zhu Q. Enhanced fluorescence diffuse optical tomography with indocyanine green-encapsulating liposomes targeted to receptors for vascular endothelial growth factor in tumor vasculature. J Biomed Opt. 2013; 18(12):126014. [PubMed: 24346856]

11. Sipkins DA, Cheresh DA, Kazemi MR, Nevin LM, Bednarski MD, Li KC. Detection of tumor angiogenesis *in vivo* by $a_v\beta_3$-targeted magnetic resonance imaging. Nat Med. 1998; 4(5):623–6. [PubMed: 9585240]

12. Winter PM, Caruthers SD, Kassner A, Harris TD, Chinen LK, Allen JS, Lacy EK, Zhang H, Robertson JD, Wickline SA, Lanza GM. Molecular imaging of angiogenesis in nascent Vx-2 rabbit tumors using a novel $a_v\beta_3$-targeted nanoparticle and 1.5 tesla magnetic resonance imaging. Cancer Res. 2003; 63(18):5838–43. [PubMed: 14522907]

13. Moreira JN, Ishida T, Gaspar R, Allen TM. Use of the post-insertion technique to insert peptide ligands into pre-formed stealth liposomes with retention of binding activity and cytotoxicity. Pharm Res. 2002; 19(3):265–9. [PubMed: 11934232]

14. Thirumamagal BT, Zhao XB, Bandyopadhyaya AK, Naranyanasamy S, Johnsamuel J, Tiwari R, Golightly DW, Patel V, Jehning BT, Backer MV, Barth RF, Lee RJ, Backer JM, Tjarks W. Receptor-targeted liposomal delivery of boron-containing cholesterol mimics for boron neutron capture therapy (BNCT). Bioconjug Chem. 2006; 17(5):1141–50. [PubMed: 16984121]

15. Bao L, Matsumura Y, Baban D, Sun Y, Tarin D. Effects of inoculation site and Matrigel on growth and metastasis of human breast cancer cells. Br J Cancer. 1994; 70(2):228–32. [PubMed: 8054270]

16. Zitvogel L, Apetoh L, Ghiringhelli F, Kroemer G. Immunological aspects of cancer chemotherapy. Nat Rev Immunol. 2008; 8(1):59–73. [PubMed: 18097448]

17. Chambon C, Clement O, Le Blanche A, Schouman-Claeys E, Frija G. Superparamagnetic iron oxides as positive MR contrast agents: *in vitro* and *in vivo* evidence. Magn Reson Imaging. 1993; 11(4):509–19. [PubMed: 8316064]

18. Imoukhuede PI, Popel AS. Quantitative fluorescent profiling of VEGFRs reveals tumor cell and endothelial cell heterogeneity in breast cancer xenografts. Cancer Med. 2014; 3(2):225–44. [PubMed: 24449499]

19. Duncan R, Seymour LW, O'Hare KB, Flanagan PA, Wedge S, Hume IC, Ulbrich K, Strohalm J, Subr V, Spreafico F, Grandi M, Ripamonti M, Farao M, Suarato A. Preclinical evaluation of polymer-bound doxorubicin. J Control Release. 1992; 19:331–46.

20. Kato Y, Onishi H, Machida Y. Efficacy of lactosaminated and intact *N*-succinylchitosan-mitomycin C conjugates against M5076 liver metastatic cancer. J Pharm Pharmacol. 2002; 54(4): 529–37. [PubMed: 11999131]
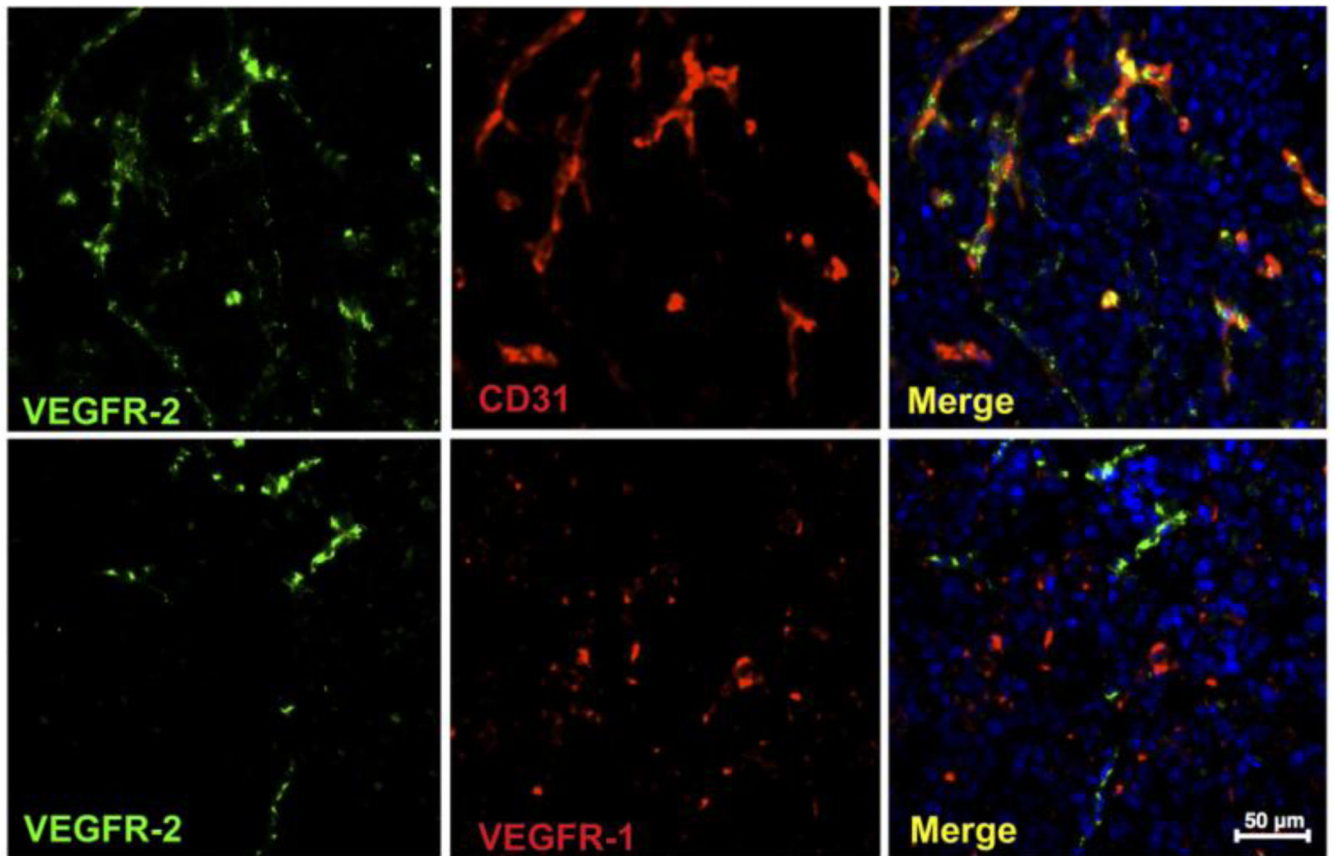
Fig. 1.
Prevalence of VEGF receptors in MDA-MB-231/luc tumors. Green: VEGFR-2; Red: Pan-endothelial marker CD31 (top) or VEGFR-1 (bottom); Blue: nuclear counterstaining with DAPI. Bar, 50 μm.
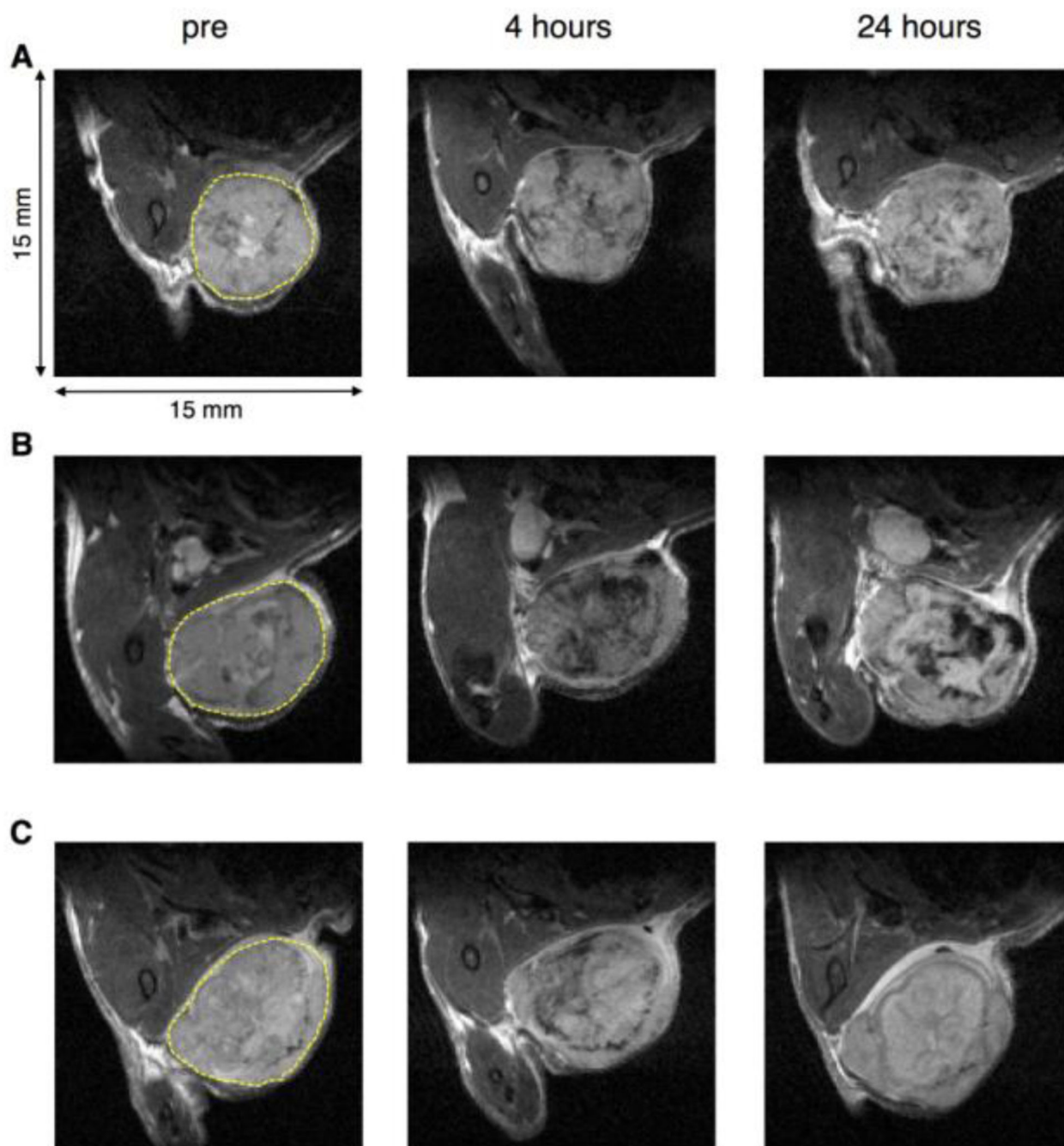
Fig. 2.
T_2-weighted MRI of MDA-MB-231/luc tumors before and after the intravenous administration of SPIONs-based contrast agents. **A**. SPIONs; **B**. Lip(Gd/Fe); **C**. scVEGF-Lip(Gd/Fe). Each yellow broken line represents a region-of-interest (ROI), in the MDA-MB-231/luc tumor. TE=35 ms.
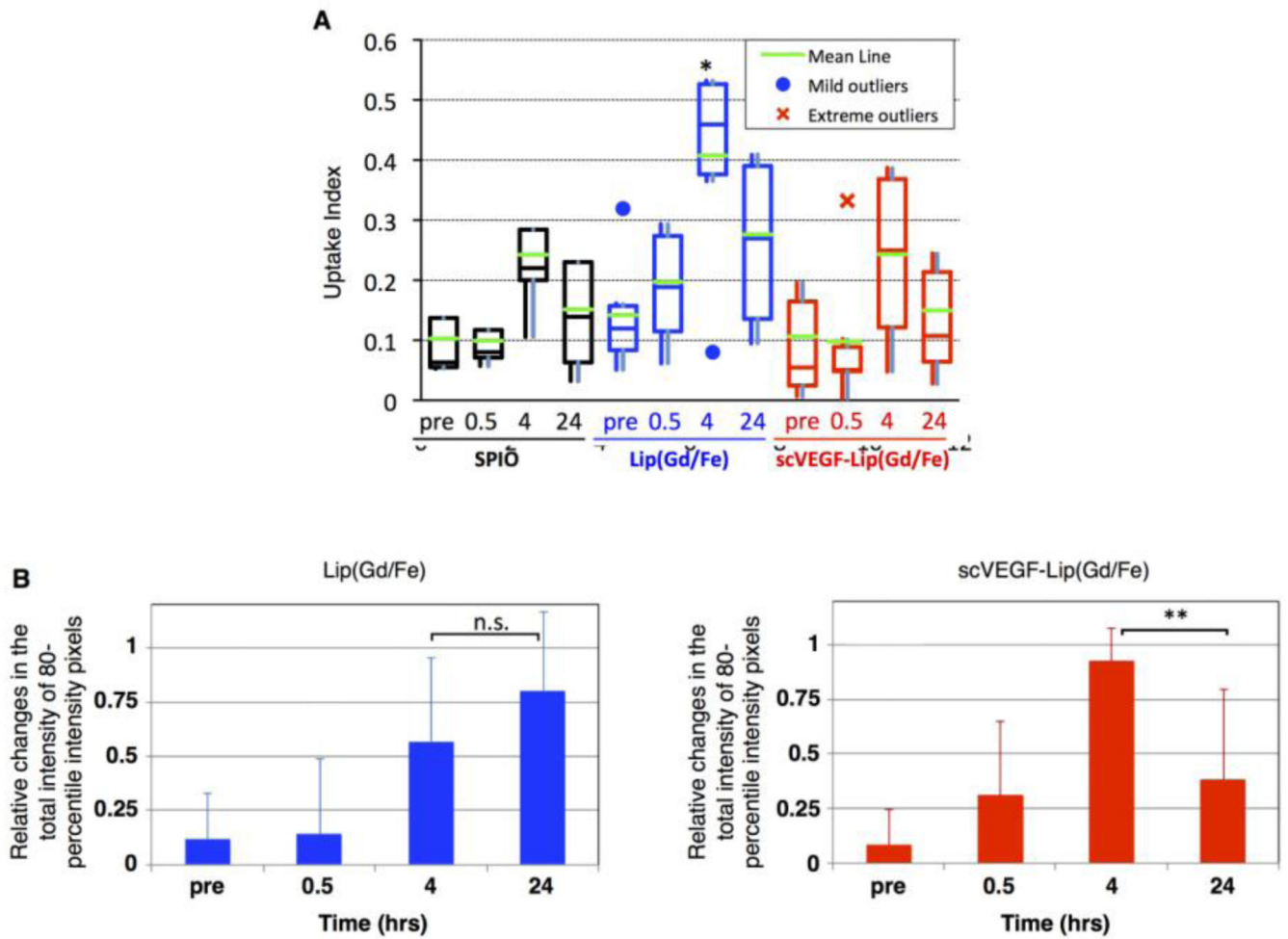
Fig. 3.
Image-based quantitative comparison of the uptake of SPIONs in an MDA-MB-231/luc tumor. **A**. Uptake index at each time point for all the groups. **B**. Relative change in the total intensity of 80th-percentile intensity pixels for Lip(Gd/Fe) and scVEGF-Lip(Gd/Fe). *: $P<0.05$. **: $P<0.01$. n.s.: Not significant.
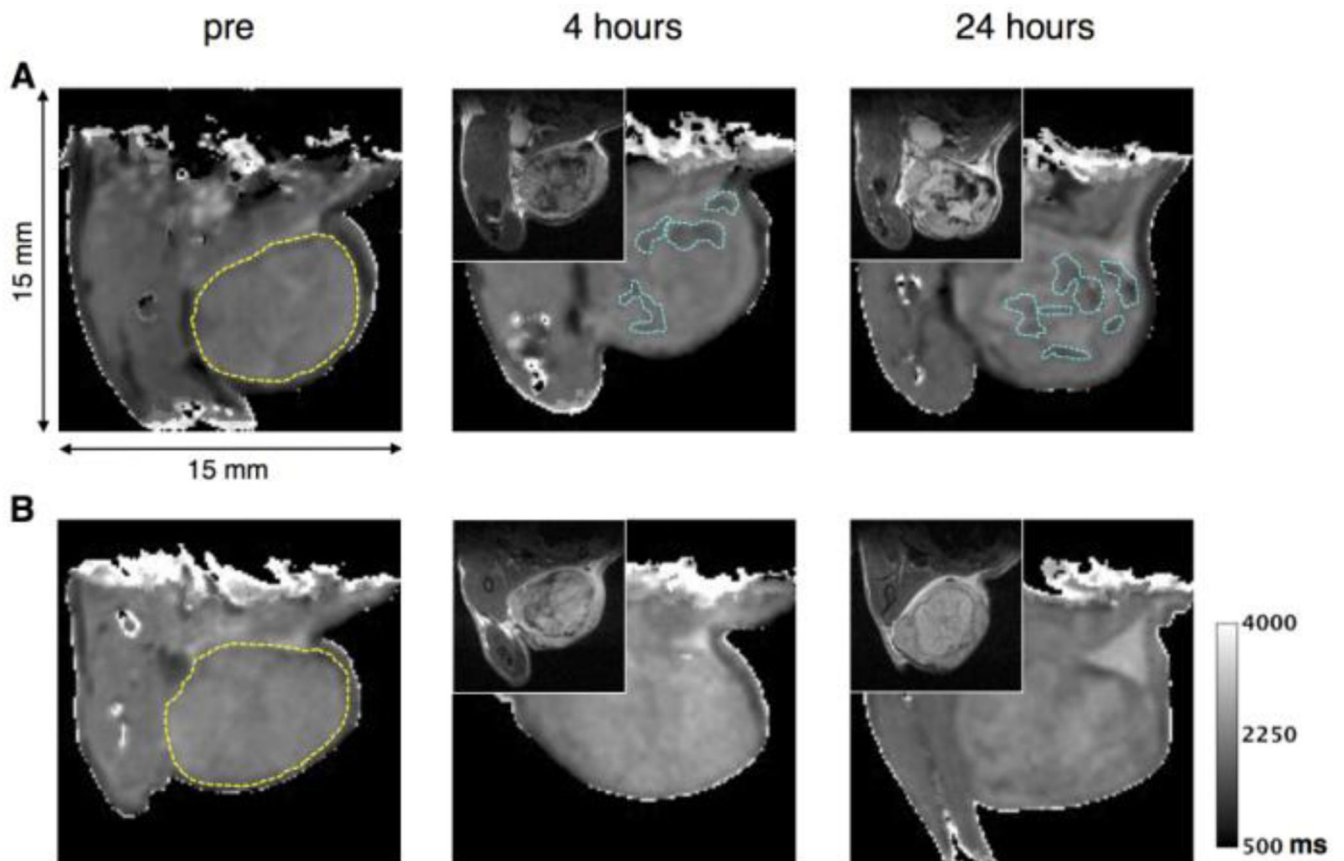
Fig. 4.
Quantitative T_1 map of MDA-MB-231/luc tumors before and after the intravenous administration of liposomes loaded with GdDTPA-BMA and SPIONs. **A**. Lip(Gd/Fe). **B**. scVEGF-Lip(Gd/Fe). Each yellow broken line represents a region-of-interest (ROI), in the MDA-MB-231/luc tumor. Blue broken lines represent the areas where SPIONs accumulated in the tumor, as detected by T_2-weighted images (inset).
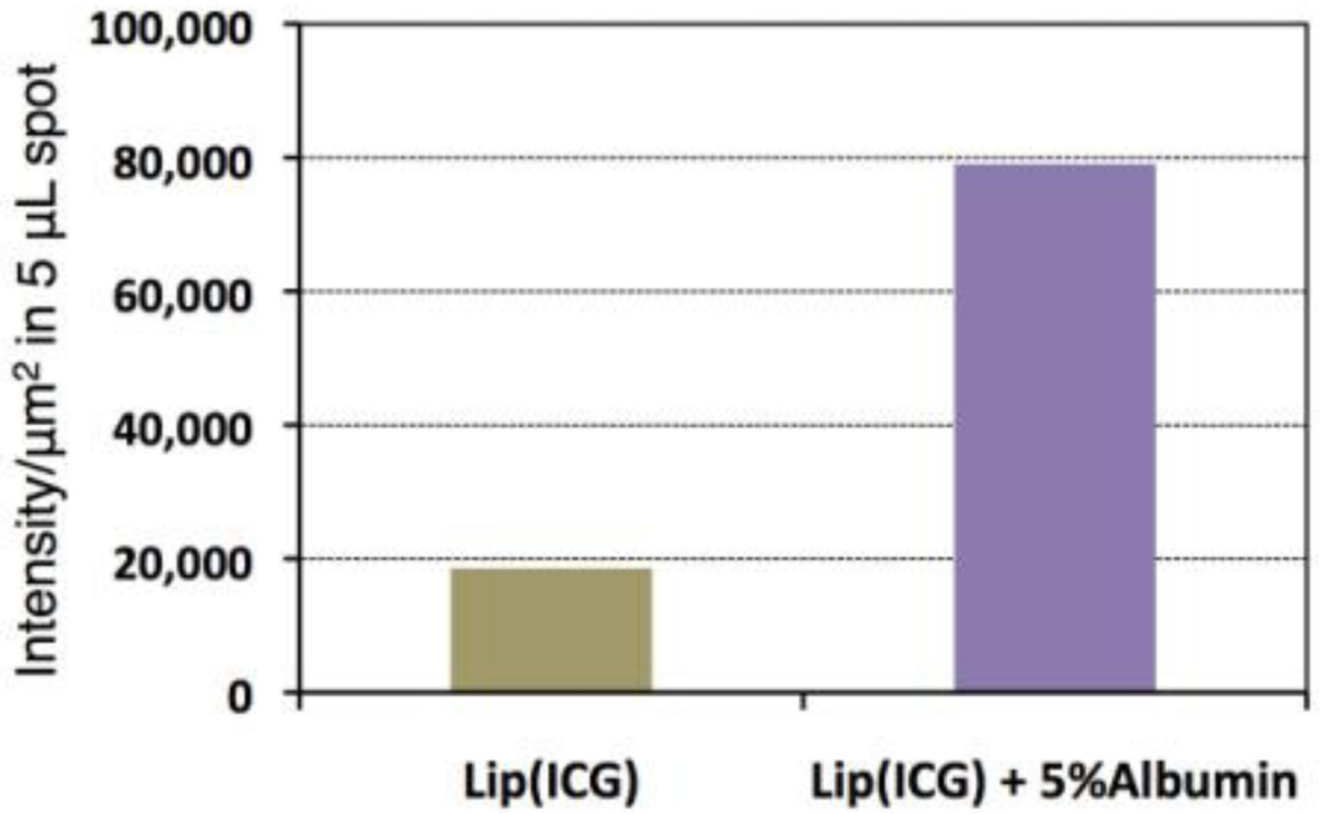
Fig. 5.
Ex vivo stability and *in vivo* tumor accumulation of Lip(ICG). Fluorescent intensity of Lip(ICG) before and after the addition of 5% human serum albumin.
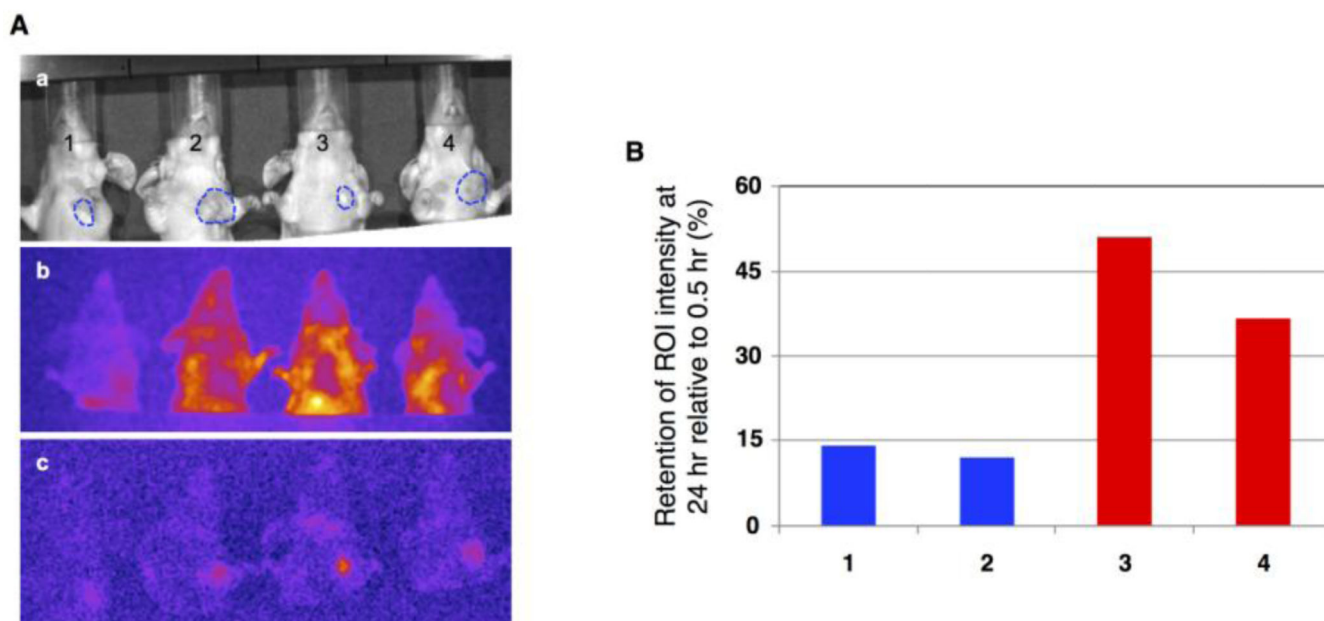
Fig. 6.
Distribution of Lip(ICG) and scVEGF-Lip(ICG) visualized by *in vivo* optical imaging. **A.**
Images of mice treated with Lip(ICG) or scVEGF-Lip(ICG). **a**. White light image. Mice #1
and #2 were injected with Lip(ICG), and mice #3 and #4 were injected with scVEGF-
Lip(ICG). Broken blue circles indicate the tumors; **b**. six hours post-injection; **c**. 24 hours
post-injection; **B**. Comparison of the accumulation of ICG in MDA-MB-231/luc tumors by
determining relative retention at 24 hours to that at 0.5 hours.
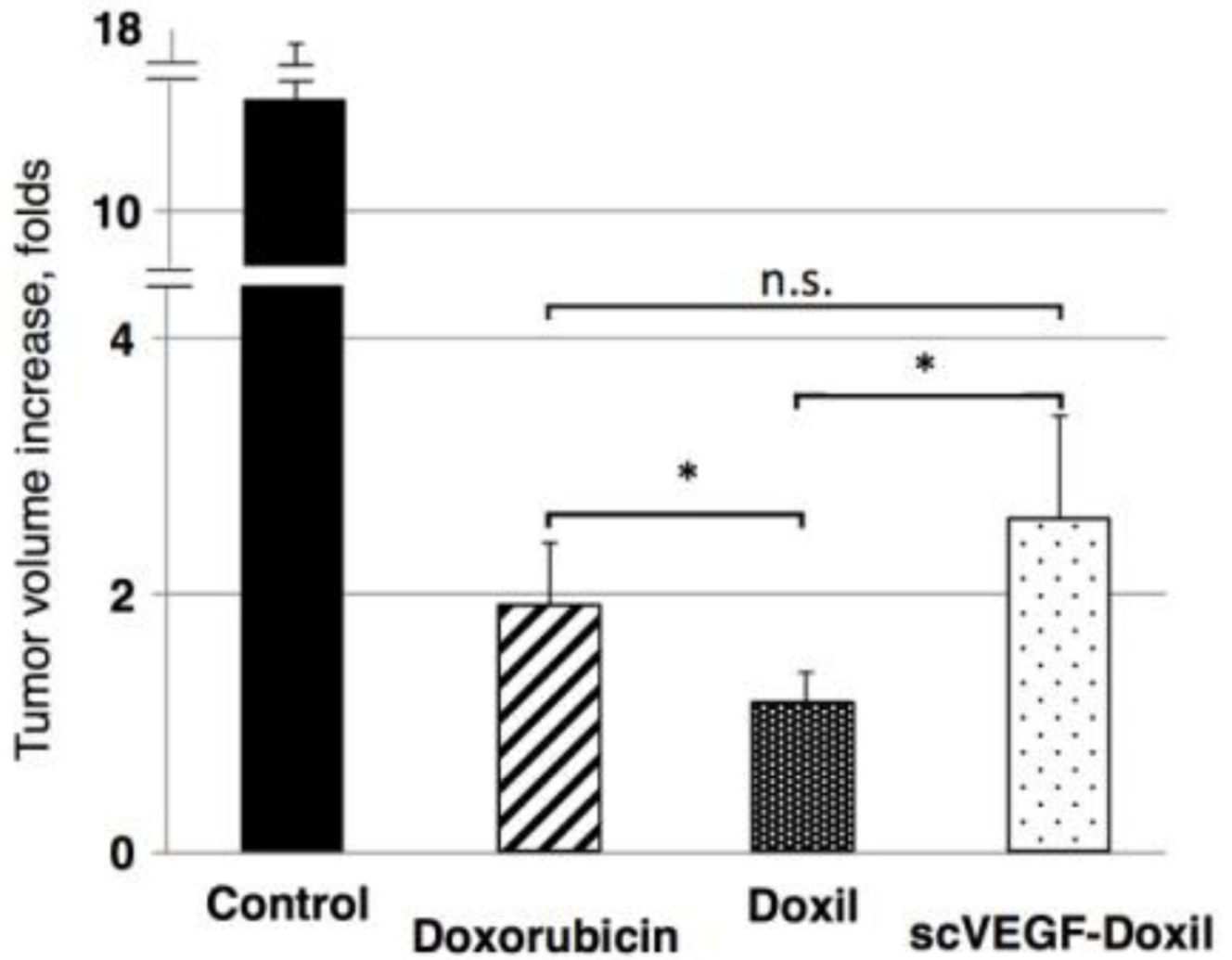
Fig. 7.
Inhibition of 4T1/luc tumor growth by free doxorubicin, Doxil®, and scVEGF-decorated Doxil® (*N*=4 for each group). n.s.: Not significant.

Table 1

Physicochemical characteristics of liposomes loaded with MRI contrast agents.

	Hydrodynamic diameter (nm)	PDI	ζ-potential (mV)	Iron concentration(μmol /mg lipid)	Gd concentration (μmol/mg lipid)
Lip(Gd/Fe)	134.7 ± 3.4	0.065 ± 0.044	−11.9 ± 0.5	9.4±7.8	35 ± 29
scVEGF-Lip(Gd/Fe)	189.0 ± 34.2	0.108 ± 0.038	−10.7 ± 1.7	3.1±2.7	3.2 ± 4.5